PHOTONICS Research

Four-wave mixing in 1.3 μm epitaxial quantum dot lasers directly grown on silicon

Jianan Duan,[1,5,†,*] Bozhang Dong,[1,†] Weng W. Chow,[2] Heming Huang,[1] Shihao Ding,[1] Songtao Liu,[3,6] Justin C. Norman,[3,7] John E. Bowers,[3] and Frédéric Grillot[1,4]

[1]LTCI, Télécom Paris, Institut Polytechnique de Paris, 91120 Palaiseau, France
[2]Sandia National Laboratories, Albuquerque, New Mexico 87185, USA
[3]Institute for Energy Efficiency, University of California Santa Barbara, Santa Barbara, California 93106, USA
[4]Center for High Technology Materials, University of New-Mexico, Albuquerque, New Mexico 87106, USA
[5]Current address: State Key Laboratory on Tunable Laser Technology, School of Electronic and Information Engineering, Harbin Institute of Technology, Shenzhen 518055, China
[6]Current address: Ayar Labs, Santa Clara, California 95054, USA
[7]Current address: Quintessent, Inc., Goleta, California 93117, USA
*Corresponding author: duanjianan@hit.edu.cn

Received 10 November 2021; revised 27 February 2022; accepted 28 February 2022; posted 1 March 2022 (Doc. ID 448082); published 21 April 2022

This work compares the four-wave mixing (FWM) effect in epitaxial quantum dot (QD) lasers grown on silicon with quantum well (QW) lasers. A comparison of theory and experiment results shows that the measured FWM coefficient is in good agreement with theoretical predictions. The gain in signal power is higher for p-doped QD lasers than for undoped lasers, despite the same FWM coefficient. Owing to the near-zero linewidth enhancement factor, QD lasers exhibit FWM coefficients and conversion efficiency that are more than one order of magnitude higher than those of QW lasers. Thus, this leads to self-mode locking in QD lasers. These findings are useful for developing on-chip sources for photonic integrated circuits on silicon.

https://doi.org/10.1364/PRJ.448082

1. INTRODUCTION

Photonic integrated circuits (PICs) on silicon can significantly advance the level of component integration and performance for both conventional and quantum information processing [1]. The advantages of silicon-based PICs are the availability of manufacturing approaches using modern nanofabrication techniques as well as the potential for miniaturization and integration of optoelectronic components with complementary functionalities [2]. In this situation, quantum dot (QD) nanostructures are a highly promising semiconductor material that can be integrated either monolithically or heterogeneously on a compact and scalable platform [3–6]. As a direct consequence of the size-confinement effect of the trapped electrons and holes, QD-based photonic devices have shown remarkable properties. In particular, epitaxial QD lasers directly grown on silicon have recently led to record performance such as ultra-low threshold currents, high temperature continuous-wave operation, very long device lifetimes, as well as high yield [3]. In addition, the use of p-doping significantly improves their thermal stability and reliability [7]. It also reduces the linewidth enhancement factor (α-factor), resulting in reflection insensitivity, which is of vital importance for isolator-free PICs [8,9]. Extending these advances to integrated photonics technologies will lead to silicon platforms with on-chip nonclassical light sources, large versatile photonic logic, quantum information storage, and highly efficient detectors [10].

Four-wave mixing (FWM) is useful in optical communications for all-optical signal processing and for wavelength-division multiplexing (WDM) systems, which are key components in coherent communication technologies [11–13]. FWM is known to drive the phase and mode locking properties observed in comb QD lasers [14–16]. Therefore, our interest in FWM coefficients involves QD lasers, where mode locking is possible with both single- and multi-section diode lasers [14,17]. In the case of WDM systems, a single-mode-locked laser producing a frequency comb can potentially replace the large number of lasers presently necessary for the task. A single-section mode-locked laser using self-mode locking amplifies the advantages even further. However, there are serious challenges because with self-mode locking, the gain medium alone has to produce the multimode lasing that leads to a broad emission bandwidth, and the FWM that contributes to locking the frequencies. Within the inhomogeneously broadened distribution of QDs, the optical nonlinearities of light–matter interactions give rise to both mechanisms. To control self-mode locking in QD lasers to the extent that it can be employed in applications, such as

WDM, a deeper understanding than we have presently of the intricate interplay of physics associated with mode competition and FWM is required. Our laser experiments and accompanying theoretical analysis are designed with exactly that goal in mind.

Within a nonlinear gain medium that has third-order nonlinear susceptibility, the beating between two co-polarized fields at different frequencies results in the occurrence of wave-mixing and the generation of two new fields. Both highly nonlinear optical fibers and high-Q micro-ring resonators are reliable solutions for efficient wave-mixing conversion. However, their limitations for monolithic integration must be addressed. For instance, the long interaction length of several meters and the strong pump power requirement make the nonlinear optical fiber not the ideal solution for a PIC [18,19]. In addition, high fabrication costs of micro-ring resonators may be another issue compared with more compact devices, such as a semiconductor optical amplifier (SOA) or semiconductor laser sources [20–22]. In the latter case, the FWM is essentially driven by carrier density pulsation (CDP), which reinforces the wave-mixing conversion efficiency; nevertheless, the nanosecond time scale of the carrier recombination lifetime leads to a slow response speed [23]. In this context, as compared to bulk and quantum well (QW) semiconductors, QD gain material is spectrally broader, and the fast carrier dynamics along with the lower α-factor improves conversion efficiency [24]. Prior work concentrated on QD SOAs [25,26] and lasers [27,28] grown on lattice matched substrates. In the former, although higher conversion efficiency can be achieved through the larger linear gain in SOAs, the inherently stronger amplified spontaneous emission noise limits the optical signal-to-noise ratio.

This paper aims at understanding FWM in QD lasers epitaxially grown on silicon, taking into account their enhanced cavity resonances and reduced amplified spontaneous emission noise. For QD systems, the basic understanding of FWM is limited by the conventional investigation method, which concentrates on the FWM coefficient measured with SOAs [25]. This work addresses this weakness by performing laser experiments to account for all optical nonlinearities contributing to the FWM signal. In our investigation, we measured and analyzed the optical nonlinearity contributions resulting in mode competition, gain saturation, carrier-induced refractive index, α-factor, and creation of combination tones, all of which have roles in self-mode locking. The experiments were performed on epitaxial QD lasers with inhomogeneous broadening below 10 meV, similar to ones that we used to achieve frequency combs with RF linewidth less than 100 kHz and mode-locked pulse below 500 fs [14]. The present motivation is to build on prior results and to confirm that the contributing nonlinearities in general combine to provide a strong mechanism of self-mode locking. To this end, we compared undoped and p-doped epitaxial QD lasers on silicon as well as a GaAs-based QW laser. GaAs-based QW lasers on Si perform poorly, so we compared to QW lasers on GaAs. A comparison with first-principles-based multimode laser theory indicates measured FWM conversion efficiencies that are close to the theoretical limit. An advantage over earlier studies and crucial to confidence in the results is the quality and reproducibility of state-of-the-art QD lasers. They make possible the detailed study of conversion efficiency over a broad parameter space, and identification of the importance of p-doping. Results reported reveal that the gain in signal power is higher for lasers with p-doped active regions than those with undoped active regions, despite the same value of FWM coefficient. Furthermore, owing to the near-zero α-factor, the measured FWM coefficient and conversion efficiency of the QD laser are more than one order of magnitude higher than those of the QW laser. This leads to stable self-mode locking in QD lasers [29]. The net FWM bandwidth of the QD laser is also twice larger than that of its QW counterpart. Overall, these findings highlight the crucial role of light emitters made with QDs for mode-locked pulses and optical frequency comb generation as well as integrated WDM technologies on silicon in future photonic integrated systems.

2. LASER DESCRIPTION

Fabry–Perot (FP) QD lasers were grown on on-axis (001) GaP/Si substrate using molecular beam epitaxy (MBE). Further details of the epitaxial growth are available elsewhere [3,7,10]. The laser structure shown in Fig. 1 includes five periods of QD layers. The dot-in-a-well QD layer composed of InGaAs QWs asymmetrically encompasses the InAs dots with a 2 nm prelayer below and a 5 nm capping layer on top. Each QD layer is separated by a 37.5 nm GaAs spacer. For p-doped QD lasers, a 10 nm p-GaAs layer at a target hole concentration of 5×10^{17} cm^{-3} (10 extra holes per QD) is sandwiched between a 10 nm undoped GaAs layer and a 17.5 nm undoped GaAs layer. We note that the gain is temperature sensitive in intrinsic QD lasers due to the thermal spreading of holes. To this problem, we introduce p-doping in the GaAs spacers. The inclusion of p-doping brings many advantages for laser devices. On one hand, p-doping can ease the thermal spread of holes and lead to rather temperature-insensitive characteristics such as threshold current, α-factor, relative intensity noise, and optical feedback resistance [11,30,31]. On the other hand, it can also eliminate

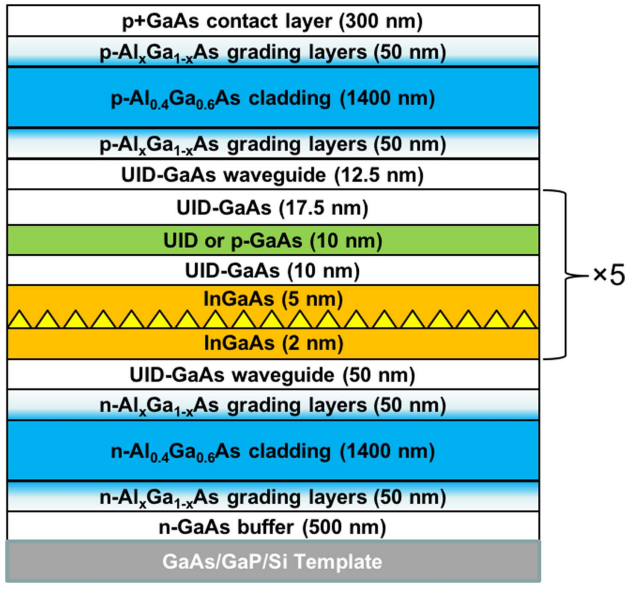

Fig. 1. Epitaxial structure of the QD laser on silicon.

gain saturation and gain broadening, hence improving the high-frequency response of QD lasers [32,33]. The undoped laser has a threshold current of 6 mA at 293 K, while the p-doped laser has a larger threshold current of 27 mA due to the high free carrier absorption caused by the large number of holes. Both QD devices emit on the sole ground state transition close to 1300 nm. Furthermore, the optimized growth conditions contribute to a narrow photoluminescence full-width-at-half-maximum below 30 meV, which transforms an inhomogeneous broadening width below 10 meV [8]. The cavity length is 1.1 mm (1.4 mm) for the undoped (p-doped) laser, which corresponds to a free spectral range (FSR) of 38 GHz (30 GHz). Both devices have a ridge waveguide width of 4 μm. The output facet has a facet coating of 60% power reflectivity while the rear facet has a value of 90%. For the QW laser counterpart, the threshold current is about 14 mA and optical gain peak is at 1277 nm. The FP cavity length is 400 μm, corresponding to a 100 GHz FSR.

3. FOUR-WAVE MIXING EXPERIMENT

The FWM experimental setup is depicted in Fig. 2 with an optical injection locking configuration. Two narrow linewidth tunable lasers are used as the drive laser and probe laser, the light of which is incorporated by a 90/10 coupler and then injected into the QD or QW laser using an optical circulator and lens-end fiber. The drive laser is used to lock the gain peak mode of FP modes, while the probe laser is used to generate the FWM with locked FP modes. Polarization controllers are applied to align the polarization of two tunable lasers with a QD or QW laser for realizing maximum conversion. The FWM optical spectrum is recorded from the optical circulator by an optical spectrum analyzer (OSA) with a 20 pm resolution. The working temperature of the QD or QW laser is kept at 293 K throughout the experiment using a thermoelectric cooler.

The probe–drive injection frequency detuning Δ is defined as the frequency difference between the drive laser and probe laser. The drive laser is used to lock the longitudinal FP mode at the gain peak while the side modes are deeply suppressed, hence generating the drive signal for wave mixing. Within the stable injection-locked regime, the frequency of the probe laser is then tuned to have the probe signal coincide with one of the suppressed FP cavity modes to obtain maximum conversion. Upconversion (downconversion) refers to the frequency of the converted signal being higher (lower) than that of the drive laser, and Δ is negative (positive). Figure 3 shows typical upconversion FWM spectra recorded for an undoped laser with $\Delta = -114$ GHz and for the p-doped laser with $\Delta = -89$ GHz as well as for QW laser with $\Delta = -110$ GHz. The middle peak represents the FP mode locked in the gain peak at the drive laser frequency with deeply suppressed sidemodes. The left peak is the probe signal mode while the right one is the wave-mixing induced converted signal mode. The different colored curves in Fig. 3 show that signal power increases with the increasing probe signal power. The FWM conversion efficiency is expressed as [24]

$$\eta_{\mathrm{CE}} = \frac{P_{\mathrm{Signal}}}{P_{\mathrm{Probe}}}, \tag{1}$$

with P_{Signal} the optical power of the converted signal and P_{Probe} the probe signal power injected into the laser. In the experiment, these modal powers are obtained from the measured optical spectrum. The laser–fiber coupling loss is estimated by calculating the ratio between laser free-space output power and the laser power coupled in the lens-end fiber. Total losses include coupling loss and fiber loss, which are considered in the spectra in order not to over-estimate the value of η_{CE}. The value of η_{CE} is expressed in logarithmic scale (in dB) in this paper.

In the first set of measurements, we keep the probe power constant, adjust the probe frequency by multiples of FSR, and record the resulting maximal η_{CE} for each FSR. Figure 4

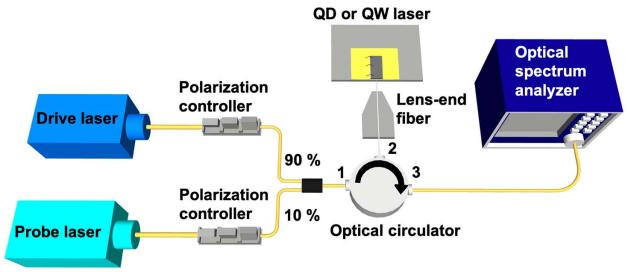

Fig. 2. Optical injection locking setup used for the four-wave mixing experiments.

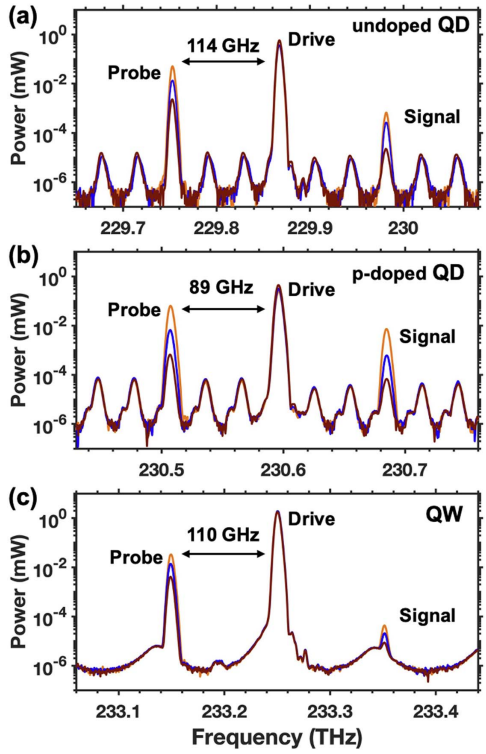

Fig. 3. Optical spectra from a four-wave mixing experiment for (a) undoped QD laser with upconversion frequency detuning of −114 GHz (probe–drive mode number difference $\Delta m = 3$); (b) p-doped QD laser with upconversion frequency detuning of −89 GHz (probe–drive mode number difference $\Delta m = 3$) and QW laser with upconversion frequency detuning of −110 GHz (probe–drive mode number difference $\Delta m = 1$). The different colored lines indicate signal power increases with increasing probe power.

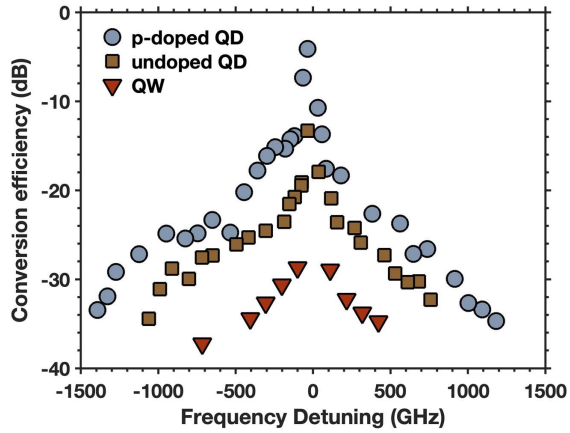

Fig. 4. Conversion efficiency of four-wave mixing for p-doped QD, undoped QD, and QW lasers as a function of probe–drive frequency detuning.

compares the measured η_{CE} for undoped QD, p-doped QD, and QW lasers as a function of probe–drive injection frequency detuning. The maximal η_{CE} is found at −13 dB for the undoped laser and −4 dB for the p-doped laser when the probe laser is injected into the first longitudinal mode next to the drive signal. These results are consistent with a native InAs/GaAs QD laser, while the maximal η_{CE} is a bit larger due to the high QD uniformity and reduced threading dislocation density [24,30]. For the undoped laser, η_{CE} is kept above −35 dB for upconversion with frequency detunings up to 1 THz and up to 760 GHz for downconversion. The frequency detunings for η_{CE} above −35 dB in the p-doped laser are larger than those of the undoped laser, which are up to 1.4 THz for upconversion and 1.2 THz for downconversion. The larger maximal η_{CE} and frequency detuning bandwidth in the p-doped laser are due to the increased material gain because p-doping reduces gain saturation and gain broadening [34]. It is noted that the static conversion at a low-frequency detuning region is determined by CDP, which is directly caused by the probe–drive beating. For larger frequency detunings, carrier heating (CH) and spectral hole burning (SHB) become the dominant mechanisms occurring within sub-picosecond time scales [26]. Although η_{CE} are higher at low-frequency detuning, hence increasing third-order nonlinear susceptibility, the very large frequency detuning bandwidth provided by CH and SHB remains very promising for broadband wavelength conversion. The different bandwidth between up- and downconversion is attributed to the asymmetry in the gain profile leading to a non-zero α-factor. In theory, with a zero α-factor, the bandwidths are perfectly symmetric. Although the α-factor is small in epitaxial QD lasers, destructive interferences still persist due to the phase condition arising between the different nonlinear processes (e.g., CDP, CH, and SHB). In addition, the profiles between upconversion and downconversion are found to be more symmetric in p-doped lasers than in undoped ones, which is due to a lower α-factor. As previously demonstrated, the α-factor of the p-doped laser is found to be as low as 0.1 at the gain peak, which is lower than that of the undoped laser with α-factor of 0.3 [30]. Compared with QD devices, the maximal η_{CE} of a QW laser is about −30 dB, which is 17 dB lower than that of an undoped laser and 26 dB lower than that of a p-doped laser. In addition, the measured FWM bandwidth of the p-doped QD laser is twice larger than that of the QW device, owing to its stronger SHB mechanism [26]. These results reveal that utilizing QDs as the active region is beneficial for providing sufficient optical nonlinearities for a laser source applied to PICs.

4. EXTRACTING FOUR-WAVE MIXING COEFFICIENT

Due to their fast carrier–carrier and carrier–phonon scatterings, QDs have shown large optical nonlinearities, and fast FWM conversion has been achieved in QD SOAs as a result of fast carrier scattering inducing deeper spectral holes [34]. The optical nonlinearities of epitaxial QD lasers on silicon and QW lasers are analyzed based on a microscopic level model containing quantum mechanical electron–hole polarization. A detailed description of QD and QW models can be found in Refs. [35,36]. Along with fitting to experimental data, we computed the signal–drive ratio using a first-principles multimode laser theory [37,38]. The signal–drive ratio η_{sd} is defined as the ratio of signal power to drive power, while the probe–drive ratio η_{pd} is the ratio of probe power to drive power. The theory gives the active medium nonlinearities contributing to gain saturation, mode competition, and multiwave mixing. In particular, it provides an analytical formula for the FWM coefficient:

$$\xi = \frac{c}{2\nu_d n_B}\left(\frac{\mathcal{P}}{2\hbar\gamma}\right)^2 \Gamma(k_d, k_p, k_s)\frac{|\Lambda^{(3)}(\nu_d, \nu_p, \nu_s)|}{\mathrm{Re}[\Lambda^{(1)}(\nu_d)]}, \tag{2}$$

where $\xi \equiv \chi^{(3)}_{\mathrm{sdpd}}/g_s$, with $\chi^{(3)}_{\mathrm{sdpd}}$ the three-order nonlinear susceptibility and g_s the material gain. c is the speed of light in vacuum, n_B is the background refractive index, $\mathcal{P}$ is the GaAs bulk dipole matrix element, and γ is the dephasing rate. Entering into Eq. (2) is spatial hole burning, including the creation of a spatial population grating, via $\Gamma(k_d, k_p, k_s)$, where k_n is the wave vector ($n = d, p, s$ for drive, probe, and signal fields, respectively). Also in Eq. (2) are the contributions from SHB and population pulsation, via $\Lambda^{(3)}(\nu_d, \nu_p, \nu_s)$, where ν_n represents the field frequencies. The magnitude of $\Lambda^{(3)}$ depends on the dephasing and population scattering rates. Last, $\Lambda^{(1)}$ is the spectral component of the linear susceptibility. Contained in $\Lambda^{(1)}$ and $\Lambda^{(3)}$ is a sum over the inhomogeneous QD distribution for the case of a QD active medium, or a sum over conduction and valence band states for a QW active medium. The detailed expression for the contribution to ξ and its input parameters are described in an earlier paper [35]. Last, Eq. (2) shows the convenience of using the FWM coefficient, because it depends only on the electronic structure and broadenings associated with carrier scattering. Its generality arises from being independent of the laser configuration, i.e., independent of confinement factor, QD density, heterostructure layer thicknesses, and injection current. The input parameters for the model are determined by anchoring computed laser behavior to measured ones such as free-running laser light–current curves and lasing spectra, as well as injection-locked laser spectra. We note that the higher intracavity absorption and

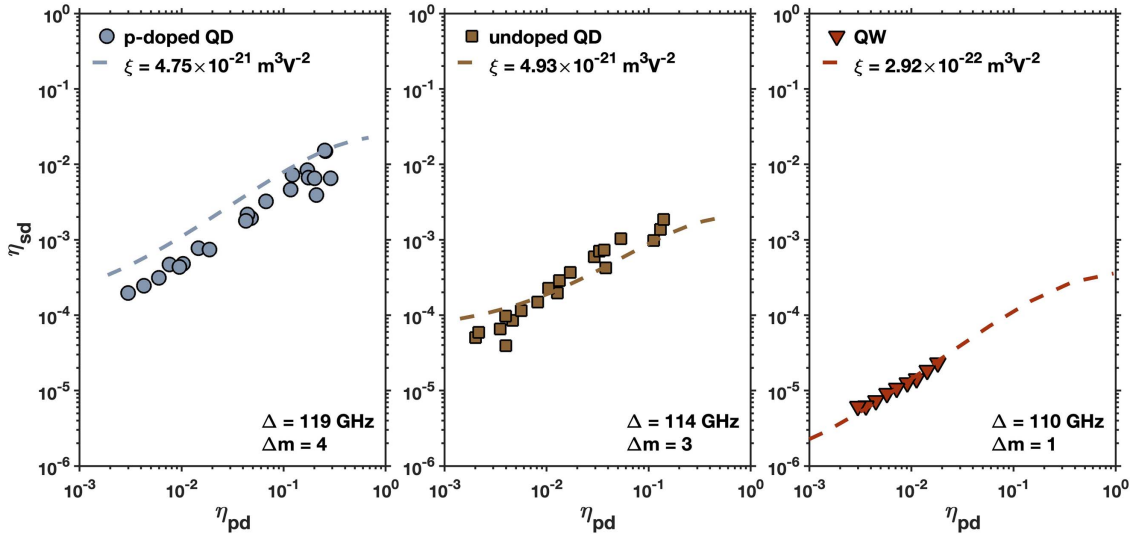

Fig. 5. Signal–drive ratio η_{sd} as a function of probe–drive ratio η_{pd} for p-doped QD, undoped QD, and QW lasers. The lasers are biased at twice threshold current. The data points are from the experiment with probe–drive injection frequency detuning Δ and probe–drive mode number difference Δm as indicated. The dashed curves are calculated from multimode laser theory indicating the corresponding FWM coefficient.

defect loss rate with p-doping are consistent with previous studies on p-doping effects [34]. The p-doping changes linear and nonlinear gain properties through state filling and carrier scattering induced dephasing, and alters the defect loss and intracavity absorption [34]. These effects are taken into account in the model.

We repeat the measurement giving the spectra in Fig. 3 for a range of probe powers. The points in Fig. 5 summarize the experimental results and show η_{sd} as a function of η_{pd}. For a fair comparison, the probe–drive injection frequency detuning for the three lasers is fixed between 110 and 120 GHz. The dashed curves are calculated from multimode laser theory indicating the corresponding FWM coefficient. The model simulations are in good agreement with experiment results. A comparison of theory and experiment indicates that the FWM coefficient from our samples is consistent with theoretical predictions. The FWM coefficient is found at 4.75×10^{-21} $m^3\,V^{-2}$ for the p-doped QD laser and 4.93×10^{-21} $m^3\,V^{-2}$ for the undoped QD laser. Within the variance of measured data, both undoped and p-doped lasers have basically the same values for ξ. However, as shown in Fig. 5, the gain in signal power with increasing probe power (slope of data points and curves) indicates higher net FWM gain with p-doping. Owing to the near-zero α-factor, the ξ and η_{sd} of QD lasers are more than one order of magnitude higher than those of the QW laser with ξ of 2.92×10^{-22} $m^3\,V^{-2}$. This high ξ results in self-mode locking of QD lasers, which was not observed for QW lasers [29].

5. CONCLUSION AND PERSPECTIVES

In conclusion, we investigated the nonlinear optical properties of QD lasers directly grown on silicon and QW lasers. Our experiments show the roles of different optical nonlinearities contributing to the demonstration of self-mode locking in QD lasers fabricated for use in silicon-based PICs. Gain saturation, mode competition, and multiwave mixing are connected through active region third-order optical nonlinearities arising from photogenerated carriers [35]. These results emphasize the need to consider linewidth enhancement effects, gain competition, and $\chi^{(3)}_{sdpd}$ on equal footing and under similar experimental conditions when evaluating mode-locking performance. Hence, caution should be exercised when drawing conclusions using only $\chi^{(3)}_{sdpd}$ measured in SOA experiments. Rather, measurements should be made directly with lasers with configurations closely resembling the lasers attempting mode locking. In contrast to SOA experiments, probe–drive laser measurements provide valuable insight into the intricate interplay of optical nonlinearities during device operation. We show that the gain in signal power with increasing probe power produces a much higher net FWM gain, the latter being even further magnified owing to p-doping. Consequently, the laser experiments provide clear differences from the SOA ones because of the gain saturation by the drive and probe intracavity fields [36]. In both theory and experiments, our results demonstrate that the optical nonlinearities in a QD gain medium are more favorable to self-mode locking. Our experiments indicate an increase of more than one order of magnitude in conversion efficiency and FWM coefficient compared to the QW device. The measured FWM bandwidth of the p-doped QD laser is twice larger than that of the QW device. Such findings provide valuable insight to understand the self-mode-locking mechanism observed from QD lasers that exclude the saturable absorber section. From a technical perspective, QD lasers exhibit unique properties for realizing self-mode locking through FWM by providing sufficient optical nonlinearities to overcome the dispersion within the laser cavity.

While epitaxial QD lasers on silicon are already strong building blocks of on-chip integrated quantum photonic circuits [39,40], further analysis could possibly extend this work to semiconductor-based quantum information systems. For

instance, the high $\chi^{(3)}_{sdpd}$ can be used for light squeezing to reduce noise below the standard quantum limit [41,42]. Squeezed states can be generated by using an FWM source made with epitaxial QDs [43,44]. Overall, these results allow us to present new insights into third order nonlinearity for the mode-locking mechanism of the QD comb laser.

Funding. Basic and Applied Basic Research Foundation of Guangdong Province (2021A1515110076); Center for Integrated Nanotechnologies, an Office of Science User Facility operated for the U.S. Department of Energy (DOE) Office of Science by Los Alamos National Laboratory (2021BC0057); DARPA PIPES (HR0011-19-C-0083).

Acknowledgment. J.D. acknowledges financial support from Guangdong Basic and Applied Basic Research Foundation and the Research Startup Fund of HITSZ.

Disclosures. J.E.B. is a cofounder of Quintessent and Nexus Photonics, silicon photonics companies.

Data Availability. All data generated or analyzed during this study are available within the paper and its supplementary materials. Further source data will be made available upon reasonable request.

Code Availability. The analysis codes will be made available upon reasonable request.

[†]These authors contributed equally to this paper.

REFERENCES

1. A. W. Elshaari, W. Pernice, K. Srinivasan, O. Benson, and V. Zwiller, "Hybrid integrated quantum photonic circuits," Nat. Photonics **14**, 285–298 (2020).
2. R. Helkey, A. A. Saleh, J. Buckwalter, and J. E. Bowers, "High-performance photonic integrated circuits on silicon," IEEE J. Sel. Top. Quantum Electron. **25**, 8300215 (2019).
3. J. C. Norman, D. Jung, Z. Zhang, Y. Wan, S. Liu, C. Shang, R. W. Herrick, W. W. Chow, A. C. Gossard, and J. E. Bowers, "A review of high-performance quantum dot lasers on silicon," IEEE J. Quantum Electron. **55**, 2000511 (2019).
4. M. Liao, S. Chen, Z. Liu, Y. Wang, L. Ponnampalam, Z. Zhou, J. Wu, M. Tang, S. Shutts, Z. Liu, P. M. Smowton, S. Yu, A. Seeds, and H. Liu, "Low-noise 1.3 μm InAs/GaAs quantum dot laser monolithically grown on silicon," Photon. Res. **6**, 1062–1066 (2018).
5. K. Nishi, K. Takemasa, M. Sugawara, and Y. Arakawa, "Development of quantum dot lasers for data-com and silicon photonics applications," IEEE J. Sel. Top. Quantum Electron. **23**, 1901007 (2017).
6. C. Zhang, D. Liang, G. Kurczveil, A. Descos, and R. G. Beausoleil, "Hybrid quantum-dot microring laser on silicon," Optica **6**, 1145–1151 (2019).
7. J. C. Norman, Z. Zhang, D. Jung, C. Shang, M. Kennedy, M. Dumont, R. W. Herrick, A. C. Gossard, and J. E. Bowers, "The importance of p-doping for quantum dot laser on silicon performance," IEEE J. Quantum Electron. **55**, 2001111 (2019).
8. F. Grillot, J. C. Norman, J. Duan, Z. Zhang, B. Dong, H. Huang, W. W. Chow, and J. E. Bowers, "Physics and applications of quantum dot lasers for silicon photonics," Nanophotonics **9**, 1271–1286 (2020).
9. J. Duan, H. Huang, B. Dong, D. Jung, J. C. Norman, J. E. Bowers, and F. Grillot, "1.3-μm reflection insensitive InAs/GaAs quantum dot lasers directly grown on silicon," IEEE Photon. Technol. Lett. **31**, 345–348 (2019).
10. J. C. Norman, D. Jung, Y. Wan, and J. E. Bowers, "Perspective: the future of quantum dot photonic integrated circuits," APL Photon. **3**, 030901 (2018).
11. W. W. Chow and F. Jahnke, "On the physics of semiconductor quantum dots for applications in lasers and quantum optics," Prog. Quantum Electron. **37**, 109–184 (2013).
12. B. Stern, X. Zhu, C. P. Chen, L. D. Tzuang, J. Cardenas, K. Bergman, and M. Lipson, "On-chip mode-division multiplexing switch," Optica **2**, 530–535 (2015).
13. Q. Cheng, M. Bahadori, M. Glick, S. Rumley, and K. Bergman, "Recent advances in optical technologies for data centers: a review," Optica **5**, 1354–1370 (2018).
14. S. Liu, D. Jung, J. Norman, M. Kennedy, A. Gossard, and J. Bowers, "490 fs pulse generation from passively mode-locked single section quantum dot laser directly grown on on-axis GaP/Si," Electron. Lett. **54**, 432–433 (2018).
15. B. Dong, H. Huang, J. Duan, G. Kurczveil, D. Liang, R. G. Beausoleil, and F. Grillot, "Frequency comb dynamics of a 1.3 μm hybrid-silicon quantum dot semiconductor laser with optical injection," Opt. Lett. **44**, 5755–5758 (2019).
16. P. Bardella, L. L. Columbo, and M. Gioannini, "Self-generation of optical frequency comb in single section quantum dot Fabry-Perot lasers: a theoretical study," Opt. Express **25**, 26234–26252 (2017).
17. X. Huang, A. Stintz, H. Li, L. Lester, J. Cheng, and K. Malloy, "Passive mode-locking in 1.3 μm two-section InAs quantum dot lasers," Appl. Phys. Lett. **78**, 2825–2827 (2001).
18. J. H. Lee, W. Belardi, K. Furusawa, P. Petropoulos, Z. Yusoff, T. M. Monro, and D. J. Richardson, "Four-wave mixing based 10-Gb/s tunable wavelength conversion using a holey fiber with a high SBS threshold," IEEE Photon. Technol. Lett. **15**, 440–442 (2003).
19. T. H. Tuan, T. Cheng, K. Asano, Z. Duan, W. Gao, D. Deng, T. Suzuki, and Y. Ohishi, "Optical parametric gain and bandwidth in highly nonlinear tellurite hybrid microstructured optical fiber with four zero-dispersion wavelengths," Opt. Express **21**, 20303–20312 (2013).
20. M. Ferrera, L. Razzari, D. Duchesne, R. Morandotti, Z. Yang, M. Liscidini, J. Sipe, S. Chu, B. Little, and D. Moss, "Low-power continuous-wave nonlinear optics in doped silica glass integrated waveguide structures," Nat. Photonics **2**, 737–740 (2008).
21. M. Ferrera, D. Duchesne, L. Razzari, M. Peccianti, R. Morandotti, P. Cheben, S. Janz, D.-X. Xu, B. Little, S. Chu, and D. J. Moss, "Low power four wave mixing in an integrated, micro-ring resonator with Q = 1.2 million," Opt. Express **17**, 14098–14103 (2009).
22. J. R. Ong, R. Kumar, R. Aguinaldo, and S. Mookherjea, "Efficient cw four-wave mixing in silicon-on-insulator micro-rings with active carrier removal," IEEE Photon. Technol. Lett. **25**, 1699–1702 (2013).
23. G. P. Agrawal, "Population pulsations and nondegenerate four-wave mixing in semiconductor lasers and amplifiers," J. Opt. Soc. Am. B **5**, 147–159 (1988).
24. H. Huang, D. Arsenijević, K. Schires, T. Sadeev, D. Erasme, D. Bimberg, and F. Grillot, "Efficiency of four-wave mixing in injection-locked InAs/GaAs quantum-dot lasers," AIP Adv. **6**, 125105 (2016).
25. T. Akiyama, H. Kuwatsuka, T. Simoyama, Y. Nakata, K. Mukai, M. Sugawara, O. Wada, and H. Ishikawa, "Nonlinear gain dynamics in quantum-dot optical amplifiers and its application to optical communication devices," IEEE J. Quantum Electron. **37**, 1059–1065 (2001).
26. H. Ishikawa, "Applications of quantum dot to optical devices," in *Semiconductors and Semimetals* (1999), Vol. **60**, pp. 287–324.
27. H. Su, H. Li, L. Zhang, Z. Zou, A. Gray, R. Wang, P. Varangis, and L. Lester, "Nondegenerate four-wave mixing in quantum dot distributed feedback lasers," IEEE Photon. Technol. Lett. **17**, 1686–1688 (2005).
28. T. Sadeev, H. Huang, D. Arsenijević, K. Schires, F. Grillot, and D. Bimberg, "Highly efficient non-degenerate four-wave mixing under dual-mode injection in InP/InAs quantum-dash and quantum-dot lasers at 1.55 μm," Appl. Phys. Lett. **107**, 191111 (2015).
29. P. J. Poole, Z. Lu, J. Liu, P. Barrios, Y. Mao, and G. Liu, "A performance comparison between quantum dash and quantum well Fabry-Pérot lasers," IEEE J. Quantum Electron. **57**, 2500207 (2021).

30. J. Duan, H. Huang, D. Jung, Z. Zhang, J. Norman, J. Bowers, and F. Grillot, "Semiconductor quantum dot lasers epitaxially grown on silicon with low linewidth enhancement factor," Appl. Phys. Lett. **112**, 251111 (2018).
31. J. Duan, Y. Zhou, B. Dong, H. Huang, J. C. Norman, D. Jung, Z. Zhang, C. Wang, J. E. Bowers, and F. Grillot, "Effect of p-doping on the intensity noise of epitaxial quantum dot lasers on silicon," Opt. Lett. **45**, 4887–4890 (2020).
32. D. G. Deppe, H. Huang, and O. B. Shchekin, "Modulation characteristics of quantum-dot lasers: The influence of p-type doping and the electronic density of states on obtaining high speed," IEEE J. Quantum Electron. **38**, 1587–1593 (2002).
33. M. T. Crowley, N. A. Naderi, H. Su, F. Grillot, and L. F. Lester, "GaAs-based quantum dot lasers," in *Semiconductors and Semimetals* (Elsevier, 2012), pp. 371–417.
34. Z. Zhang, D. Jung, J. C. Norman, P. Patel, W. W. Chow, and J. E. Bowers, "Effects of modulation p doping in InAs quantum dot lasers on silicon," Appl. Phys. Lett. **113**, 061105 (2018).
35. W. W. Chow, S. Liu, Z. Zhang, J. E. Bowers, and M. Sargent, "Multimode description of self-mode locking in a single-section quantum-dot laser," Opt. Express **28**, 5317–5330 (2020).
36. F. Grillot, J. Duan, B. Dong, H. Huang, S. Liu, W. Chow, J. Norman, and J. Bowers, "Quantum dot lasers based photonics integrated circuits," in *IEEE Photonics Conference (IPC)* (IEEE, 2020), pp. 1–2.
37. M. Sargent III, M. Scully, and W. Lamb, Jr., *Laser Physics* (Addison-Wesley, 1974).
38. D. Nielsen and S. L. Chuang, "Four-wave mixing and wavelength conversion in quantum dots," Phys. Rev. B **81**, 035305 (2010).
39. G. Moody, L. Chang, T. J. Steiner, and J. E. Bowers, "Chip-scale nonlinear photonics for quantum light generation," AVS Quantum Sci. **2**, 041702 (2020).
40. T. J. Steiner, J. E. Castro, L. Chang, Q. Dang, W. Xie, J. Norman, J. E. Bowers, and G. Moody, "Ultrabright entangled-photon-pair generation from an AlGaAs-on-insulator microring resonator," PRX Quantum **2**, 010337 (2021).
41. F. Jérémie, C. Chabran, and P. Gallion, "Room-temperature generation of amplitude-squeezed light from 1550-nm distributed-feedback semiconductor lasers," J. Opt. Soc. Am. B **16**, 460–464 (1999).
42. J.-L. Vey and P. Gallion, "Semiclassical model of semiconductor laser noise and amplitude noise squeezing. II. Application to complex laser structures," IEEE J. Quantum Electron. **33**, 2105–2110 (1997).
43. Z. Qin, J. Jing, J. Zhou, C. Liu, R. C. Pooser, Z. Zhou, and W. Zhang, "Compact diode-laser-pumped quantum light source based on four-wave mixing in hot rubidium vapor," Opt. Lett. **37**, 3141–3143 (2012).
44. Y. Zhao, Y. Okawachi, J. K. Jang, X. Ji, M. Lipson, and A. L. Gaeta, "Near-degenerate quadrature-squeezed vacuum generation on a silicon-nitride chip," Phys. Rev. Lett. **124**, 193601 (2020).